Relativistic treatment of pion wave functions in the annihilation $\bar{p}p \to \pi^-\pi^+$

B. El-Bennich* and W. M. Kloet
Department of Physics and Astronomy, Rutgers University, 136 Frelinghuysen Road, Piscataway, New Jersey 08854-8019, USA
(Received 16 March 2004; published 15 September 2004)

Quark model intrinsic wave functions of highly energetic pions in the reaction $\bar{p}p \to \pi^-\pi^+$ are subjected to a relativistic treatment. The annihilation is described in a constituent quark model with $A2$ and $R2$ flavor-flux topology, and the annihilated quark-antiquark pairs are in $^3P_0$ and $^3S_1$ states. We study the effects of pure Lorentz transformations on the antiquark and quark spatial wave functions and their respective spinors in the pion. The modified quark geometry of the pion has considerable impact on the angular dependence of the annihilation mechanisms.

DOI: 10.1103/PhysRevC.70.034001 PACS number(s): 13.75.Cs, 12.39.Jh, 21.30.Fe, 25.43.+t

I. INTRODUCTION

The LEAR experiments [1] on $\bar{p}p \to \pi^-\pi^+$ and $\bar{p}p \to K^-K^+$, which yielded a large and very accurate dataset for differential cross sections $d\sigma/d\Omega$ and analyzing powers A_{0n} from 360 to 1550 MeV/c, have until very recently [2] resisted a satisfying comparison with theoretical models. In particular, the observable A_{0n} exhibits a characteristic double-dip structure which is hard to reproduce. Another prominent feature of the A_{0n} data is a shift of the asymmetry from predominantly negative values at lower momenta toward positive values at higher momenta. As already mentioned in [2,3], this indicates the presence of several partial waves while most model calculations [4–9] lead to amplitudes dominated by total angular momentum $J=0$ and $J=1$. The reason for this feature of all models is a rather short range annihilation mechanism, driven either by baryonic exchange in the t channel [4–6,9] or by overlap of quark and antiquark wave functions of the proton and antiproton as in [7,8]. We should mention however that there is another interesting possibility of coupling, for example, $J=2,3$ initial $\bar{N}N$ states to $L=0$ intermediate $\bar{N}\Delta, \bar{\Delta}N$, or $\bar{\Delta}\Delta$ states, which then can decay into mesons by a short range annihilation mechanism. This approach was investigated for total annihilation cross sections in [10,11] but not pursued for differential cross sections.

One way to improve models would hence be to increase the annihilation range. In Ref. [2], this problem is addressed within the framework of a constituent quark model. For a summary of the $\bar{p}p$ annihilation in a quark model, see the review by Dover *et al.* [12]. In paper [2], the radii of the proton, antiproton, and pion were readjusted so they coincide with the ones obtained from measurements of the respective electric form factors [13,14] rather than with the considerably smaller constituent qqq and $\bar{q}q$ quark core radii. The latter radii, which ignore the hadronic $\bar{q}q$ cloud, were used in earlier attempts to reproduce the LEAR observables [7,8]. In the model calculations, this increase in radius is directly related to the Gaussian description of the intrinsic quark wave functions. In the overlap integral over the quark coordinates, the wider Gaussian wave functions provide in turn a larger overlap of the quarks and antiquarks and therefore a larger range of the annihilation mechanism. In fact, the radii in Ref. [2] were obtained in a fit to $d\sigma/d\Omega$ and A_{0n} data mentioned above and are about 7% larger than the charge radii derived from the electric form factors. This effect, along with a fine-tuned final-state interaction of the $\pi^-\pi^+$ pair, improves the reproduction of the observables $d\sigma/d\Omega$ and A_{0n}, and in particular of the double-dip structure of the latter one, considerably.

As was pointed out in Ref. [2], there is another reason to believe that the geometry of the final pions is relevant to higher partial wave ($J>1$) contributions to the total amplitude. At the center-of-mass (c.m.) energies $\sqrt{s}$ considered in the LEAR experiment $\bar{p}p \to \pi^-\pi^+$, final pions are produced with kinetic energies much larger than the pion rest mass. For example, for an antiproton beam with $p_{\rm lab}=800$ MeV/c the total c.m. energy is $E_{\rm c.m.}=\sqrt{s}\simeq 2020$ MeV. This translates into a relativistic factor $\gamma=E_{\rm c.m.}/2m_\pi c^2=7.2$. In the quark model, the pions are described by Gaussian spheres in the rest frame of each pion. Yet, the transition amplitudes and implicitly the observables of the $\bar{p}p \to \pi^-\pi^+$ reaction are calculated in the c.m. frame. In the c.m. frame the outgoing pions, due to their large kinetic energy, will be shaped like pancakes. This will alter the angular dependence of the annihilation mechanism.

This modification of the pions, due to Lorentz transformed Gaussian wave functions, was investigated previously by Maruyama *et al.* [15] in the annihilation of $\bar{p}p$ atoms at rest into two mesons. The authors of Ref. [15] found that the two-pion production is enhanced upon including Lorentz contraction effects. However, only branching ratios were discussed, and the impact of these Lorentz contractions on the angular dependence of the annihilation $\bar{p}p \to \pi^-\pi^+$ at positive energies remained unknown.

In this paper, we will show that the pion deformation affects the overlap of intrinsic pion, proton, and antiproton wave functions. It was in this spirit that in Ref. [2] the width of the Gaussian wave function was increased not merely to reproduce the measured charge radii, but also to mock up an altered overlap of the quarks and antiquarks implied by relativistic considerations. In the following, we will carry out the Lorentz transformation which is a twofold task: the pions are

*Electronic address: bennich@physics.rutgers.edu

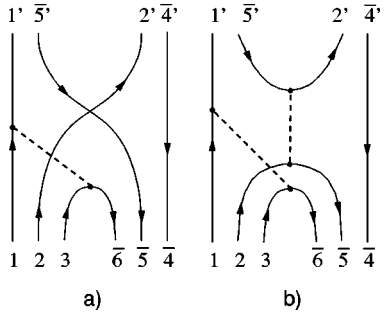

FIG. 1. (a) Rearrangement diagram $R2$ and (b) annihilation diagram $A2$. The numbers with bars denote antiquarks, those without bars the quarks, while the dashed lines represent the exchange of either the effective "vacuum" $^3P_0$ or "gluon" $^3S_1$ state.

$\overline{qq}$ pairs described by the usual spinors of the free Dirac equation times a radial Gaussian function to account for their confinement within the pion. Hence, the Lorentz transformation is effected on both spin and Gaussian components of the wave functions. Using the relevant Feynman diagrams, we analyze the relativistic effects on the amplitudes and compare them with previous results [7]. In the following we refer to two-pion final states only, however all results derived in this paper are also valid for the reaction $\overline{pp}\to K^-K^+$.

II. LORENTZ TRANSFORMED PION INTRINSIC WAVE FUNCTIONS

The reaction $\overline{pp}\to\pi^-\pi^+$ is described in the c.m. frame $S_{\text{c.m.}}$. Therefore, given the large kinetic energy of the final-state pions, we must Lorentz transform each pion intrinsic wave functions from the pion rest frame S_π to the c.m. frame $S_{\text{c.m.}}$. As mentioned before, this will affect the Gaussian radial part of the wave function which will be distorted along the boost direction into an ellipsoid. We begin with an r-space realization of the pion wave function $\psi_\pi(\mathbf{r}_1,\mathbf{r}_5)$ and first concentrate on its spatial component. In the pion rest-frame $\psi_\pi(\mathbf{r}_1,\mathbf{r}_5)$ has the form

$$\psi_\pi(\mathbf{r}_1,\mathbf{r}_5)=N_\pi\exp\left\{-\frac{\beta}{2}\sum_{i=1,5}(\mathbf{r}_i-\mathbf{R}_\pi)^2\right\}\times\chi_\pi(\text{spin},\text{isospin},\text{color}). \tag{1}$$

Following the labeling of the first pion in Fig. 1, here $\mathbf{r}_1$ and $\mathbf{r}_5$ are the quark and antiquark coordinates, respectively. The coordinate of the pion is $\mathbf{R}_\pi$. All quark and antiquark masses are assumed to be equal. For the second pion the quark and antiquark coordinates would be $\mathbf{r}_2$ and $\mathbf{r}_4$.

The proton and antiproton are described in their respective rest frames by similar Gaussian functions

$$\psi_p(\mathbf{r}_1,\mathbf{r}_2,\mathbf{r}_3)=N_p\exp\left\{-\frac{\alpha}{2}\sum_{i=1}^{3}(\mathbf{r}_i-\mathbf{R}_p)^2\right\}\times\chi_p(\text{spin},\text{isospin},\text{color}), \tag{2}$$

where $\mathbf{r}_i$ are the quark (antiquark) coordinates and $\mathbf{R}_p$ the nucleon (antinucleon) coordinate. Because of the much smaller kinetic energy and larger mass of the nucleon and antinucleon, their intrinsic distortions in $S_{\text{c.m.}}$ are ignored.

Returning to the pion, the antiquark and quark coordinates r in S_π are related to coordinates r' in $S_{\text{c.m.}}$ according to the inverse Lorentz transformation $[l^{-1}\equiv l^{-1}(\boldsymbol{\beta})]$

$$r'=l^{-1}r. \tag{3}$$

We split the quark and antiquark coordinates into components parallel and perpendicular to the boost direction $\boldsymbol{\beta}=\mathbf{v}/c$, which is related to the relativistic boost factor $\gamma=(1-\beta^2)^{-1/2}=E_{\text{c.m.}}/2m_\pi c^2$. Hence, the parallel component of the separation $\mathbf{r}_1-\mathbf{r}_5$ between an antiquark-quark pair in the pion rest frame is related to the one in the c.m. frame with coordinates $\mathbf{r}_1'$ and $\mathbf{r}_5'$ by

$$(\mathbf{r}_1-\mathbf{r}_5)_\parallel^2=\gamma^2(\mathbf{r}_1'-\mathbf{r}_5')_\parallel^2. \tag{4}$$

Here, we have used the equal time condition $t_1'=t_5'$ in the c.m. frame $S_{\text{c.m.}}$. These transformations can be applied straightforwardly to the spatial part of the pion wave functions. Inserting the Lorentz contraction of Eq. (4) in Eq. (1), the pion wave function suppressing spin, isospin, and color dependence becomes

$$\psi_\pi(l^{-1}\mathbf{r}_1,l^{-1}\mathbf{r}_5)=\tilde{N}_\pi\exp\left\{-\frac{\beta}{2}\sum_{i=1,5}\times[(\mathbf{r}_i-\mathbf{R}_\pi)_\perp^2+\gamma^2(\mathbf{r}_i-\mathbf{R}_\pi)_\parallel^2]\right\}, \tag{5}$$

where β is in this case the size parameter and $\mathbf{R}_\pi=\frac{1}{2}(\mathbf{r}_1+\mathbf{r}_5)$ is the pion coordinate. The new normalization factor $\tilde{N}_\pi=\sqrt{\gamma}N_\pi$ comes from the condition that Eq. (5) be normalized to unity in the c.m. In Eq. (5), the spatial distortion of the pions in the c.m. of the reaction $\overline{pp}\to\pi^-\pi^+$ alluded to in the Introduction is shown explicitly.

In p space the wave function is

$$\begin{aligned}\psi_\pi(l^{-1}\mathbf{p}_1,l^{-1}\mathbf{p}_5)&=\tilde{N}_\pi(4\pi/\beta)^{3/2}/\gamma\\&\times\exp-\left\{\frac{1}{2\beta}\sum_{i=1,5}\left[\left(\mathbf{p}_i-\frac{1}{2}\mathbf{P}_\pi\right)_\perp^2+\frac{1}{\gamma^2}\left(\mathbf{p}_i-\frac{1}{2}\mathbf{P}_\pi\right)_\parallel^2\right]\right\}\\&=\frac{N_\pi}{\gamma^{1/2}}\left(\frac{4\pi}{\beta}\right)^{3/2}\exp\left\{-\frac{1}{4\beta}\left[(\mathbf{p}_1-\mathbf{p}_5)^2+\left(\frac{1}{\gamma^2}-1\right)([\mathbf{p}_1-\mathbf{p}_5]\cdot\hat{\mathbf{P}}_\pi)^2\right]\right\}.\end{aligned} \tag{6}$$

The momenta $\mathbf{p}_1$ and $\mathbf{p}_5$ are the quark and antiquark momenta, while $\mathbf{P}_\pi=\mathbf{p}_1+\mathbf{p}_5$ is the pion momentum which is parallel to the boost direction. With these Lorentz transformed wave functions, we are now in the position to evaluate the $^3S_1$ and $^3P_0$ amplitudes taking into account the boosted pions. We will consider two types of commonly used diagrams, the *rearrangement* $R2$ and *annihilation* $A2$ diagrams as depicted in Fig. 1.

III. EFFECTS OF DEFORMED PIONS ON THE ANNIHILATION AMPLITUDES

With the Lorentz transformed pion intrinsic wave functions, we can recalculate the T matrix elements of Refs. [7,8] for the annihilation reaction $\bar{p}p \to \pi^-\pi^+$. Here, we will do this first for the $R2$ diagrams (which we used exclusively in a previous paper [2]). The transition operators $T(^3P_0)$ and $T(^3S_1)$ are obtained from integrating out the quark and antiquark momenta. The momenta of p, $\bar{p}$, π^-, and π^+ will be called $\mathbf{P}_p$, $\mathbf{P}_{\bar{p}}$, $\mathbf{P}_{\pi^-}$, and $\mathbf{P}_{\pi^+}$, respectively. For the $R2$ diagram of Fig. 1(a), the transition operators for the $^3P_0$ as well as the $^3S_1$ case are obtained, using the quark and antiquark labeling in diagram Fig. 1(a) and pion, antiproton, and proton wave functions of Eq. (6) and the Fourier transform of Eq. (2), from the following integral:

$$\begin{aligned}\hat{T}_{R2}(^3P_0,{}^3S_1) = \mathcal{N}\int & d\mathbf{p}_1 d\mathbf{p}_2 d\mathbf{p}_3 d\mathbf{p}_4 d\mathbf{p}_5 d\mathbf{p}_6 d\mathbf{p}_{1'} d\mathbf{p}_{2'} d\mathbf{p}_{4'} d\mathbf{p}_{5'} \delta(\mathbf{p}_{1'}+\mathbf{p}_{5'}-\mathbf{P}_{\pi^-})\delta(\mathbf{p}_{2'}+\mathbf{p}_{4'}-\mathbf{P}_{\pi^+})\delta(\mathbf{p}_1+\mathbf{p}_2+\mathbf{p}_3-\mathbf{P}_p)\\
&\times\delta(\mathbf{p}_4+\mathbf{p}_5+\mathbf{p}_6-\mathbf{P}_{\bar{p}})\delta(\mathbf{p}_6+\mathbf{p}_3+\mathbf{p}_1-\mathbf{p}_{1'})\delta(\mathbf{p}_{2'}-\mathbf{p}_2)\delta(\mathbf{p}_{4'}-\mathbf{p}_4)\delta(\mathbf{p}_{5'}-\mathbf{p}_5)\\
&\times\exp\left\{-\frac{1}{4\beta}\left[(\mathbf{p}_{1'}-\mathbf{p}_{5'})^2+(\mathbf{p}_{2'}-\mathbf{p}_{4'})^2+\left(\frac{1}{\gamma^2}-1\right)\{[(\mathbf{p}_{2'}-\mathbf{p}_{4'})\cdot\hat{\mathbf{P}}_\pi]^2+[(\mathbf{p}_{1'}-\mathbf{p}_{5'})\cdot\hat{\mathbf{P}}_\pi]^2\}\right]\right\}\\
&\times\exp\left\{-\frac{1}{2\alpha}\left(\sum_{i=1}^{3}\left(\mathbf{p}_i-\frac{1}{3}\mathbf{P}_p\right)^2+\sum_{i=4}^{6}\left(\mathbf{p}_i-\frac{1}{3}\mathbf{P}_{\bar{p}}\right)^2\right)\right\}\hat{V}_{R2}(^3P_0,{}^3S_1),\end{aligned} \tag{7}$$

where the overall normalization $\mathcal{N}$ contains factors due to the relativistic factor γ, the normalization factors N_π, N_p, $N_{\bar{p}}$, the pion size parameter β, and the proton (antiproton) size parameter α.

The two mechanisms differ only in the operators $\hat{V}_{R2}(^3P_0)$ and $\hat{V}_{R2}(^3S_1)$ stemming from the respective annihilation mechanisms

$$\hat{V}_{R2}(^3P_0) = \lambda_{R2P}\boldsymbol{\sigma}_{63}\cdot(\mathbf{p}_6-\mathbf{p}_3), \tag{8}$$

$$\hat{V}_{R2}(^3S_1) = \lambda_{R2S}[-2\boldsymbol{\sigma}_{63}\cdot\mathbf{p}_1+i(\boldsymbol{\sigma}_{1'1}\times\boldsymbol{\sigma}_{63})\cdot(\mathbf{p}_1-\mathbf{p}_{1'})]. \tag{9}$$

Here λ_{R2P} and λ_{R2S} are strength parameters of the two $R2$ mechanisms.

The exponential parts in Eq. (7) originate in the p-space component of the boosted pion wave functions of Eq. (6) and the baryonic (nonboosted) wave functions of Eq. (2). The spin-momentum dependency in Eqs. (8) and (9) comes from the computation of the $R2$ diagrams using the Dirac spinors. The indices on the Pauli matrices denote the spinor subspace in which they act. For instance, the antiquark-quark pair $\bar{q}_6 q_3$ is annihilated and momentum $\mathbf{p}_3+\mathbf{p}_6$ is transferred from this vertex to quark q_1.

After Fourier transform into r space, Eq. (7) becomes for the $^3P_0$ mechanism

$$\begin{aligned}\hat{T}_{R2}(^3P_0) = i\mathcal{N}[&A_V\boldsymbol{\sigma}\cdot\mathbf{R}'+B_V\boldsymbol{\sigma}\cdot\mathbf{R}+C_V(\boldsymbol{\sigma}\cdot\hat{\mathbf{R}}')R\cos\theta]\\
&\times\exp\{AR'^2+BR^2+CRR'\cos\theta+DR^2\cos^2\theta\}.\end{aligned} \tag{10}$$

The various coefficients will be given below. Since the $^3S_1$ mechanism in Eq. (9) contains two terms, we split their contributions conveniently into a *longitudinal* and a *transversal* part. It will be seen that they give rise to different selection rules. The transition operator is thus

$$\begin{aligned}\hat{T}_{R2}(^3S_1) = \mathcal{N}[&A_L i\boldsymbol{\sigma}\cdot\mathbf{R}'+B_L i\boldsymbol{\sigma}\cdot\mathbf{R}+C_L i\boldsymbol{\sigma}\cdot\hat{\mathbf{R}}'R\cos\theta\\
&+A_T\boldsymbol{\sigma}\cdot\mathbf{R}'+B_T\boldsymbol{\sigma}\cdot\mathbf{R}+C_T(\boldsymbol{\sigma}\cdot\hat{\mathbf{R}}')R\cos\theta]\\
&\times\exp\{AR'^2+BR^2+CRR'\cos\theta+DR^2\cos^2\theta\}.\end{aligned} \tag{11}$$

The relative $\pi^-\pi^+$ and antiproton-proton coordinates are $\mathbf{R}'=\mathbf{R}_{\pi^-}-\mathbf{R}_{\pi^+}$ and $\mathbf{R}=\mathbf{R}_{\bar{p}}-\mathbf{R}_p$, respectively. The angle θ is between the relative $\pi^-\pi^+$ coordinate $\mathbf{R}'$ and antiproton-proton coordinate $\mathbf{R}$ in the c.m. system. Compared with the results of Ref. [7], one observes the appearance of additional terms in both transition operators, namely, the D term in the exponent and the C_V, C_L, and C_T terms. These new terms introduce manifest angular dependence. More precisely, the boosted pion wave functions lead to additional angular dependence in the form of quadratic cosine terms in the exponentials and linear cosine terms in the coefficients of the spin operators. Note that aside from the explicit nonlocality, the transition operators $\hat{T}_{R2}(^3P_0)$ and $\hat{T}_{R2}(^3S_1)$ are now energy dependent via the Lorentz boost factor γ. This γ dependence is nontrivial, and affects the angular dependence of the transition operators in the sense that the various terms mentioned above behave differently for increasing values of γ. Also, the magnitude of these terms differs immensely depending on whether γ is small ($\gamma\simeq 1-2$) or large ($\gamma\simeq 5-8$). For large γ the D term dominates the exponential part and, for example, $C_V \gg A_V, B_V$ and $C_L \gg A_L, B_L$; however, C_T, A_T, and B_T are of the same order of magnitude.

The above results for the transition operators are valid for the diagram in Fig. 1(a). Summing over all possible permutations of Fig. 1(a), where for example $\mathbf{p}_3+\mathbf{p}_6$ is transferred to quark q_2 or one of the antiquarks $\bar{q}_4, \bar{q}_5$, yields the same symmetry properties as in Ref. [7], as expected. In particular, the *vacuum* coefficients A_V, B_V, and C_V add up such that $\hat{T}_{R2}(^3P_0)$ contributes only to $l_{\pi\pi}=0,2,4,\ldots$ and $l_{\bar{p}p}=1,3,5,\ldots$ and hence acts in $\bar{p}p$ states with $J^\pi=0^+,2^+,4^+,\ldots$ waves. The longitudinal part of the transition amplitude $\hat{T}_{R2}(^3S_1)$, with the coefficients A_L, B_L, and C_L, bears the same symmetry properties and therefore acts in the same waves as the "vacuum" mechanism. The transversal component with A_T, B_T, and C_T, on the other hand, contributes to $l_{\pi\pi}=1,3,5,\ldots$ and $l_{\bar{p}p}=0,2,4,\ldots$ and acts therefore in $\bar{p}p$ states with $J^\pi=1^-,3^-,5^-,\ldots$ waves.

The complete form of the $R2$ transition operators for the vacuum $^3P_0$ amplitude when summing over all permutations is

$$\begin{aligned}\hat{T}^{\mathrm{tot}}_{R2}(^3P_0) = i\mathcal{N}[&A_V\boldsymbol{\sigma}\cdot\mathbf{R}'\sinh(C\mathbf{R}\cdot\mathbf{R}')\\ &+B_V\boldsymbol{\sigma}\cdot\mathbf{R}\cosh(C\mathbf{R}\cdot\mathbf{R}')\\ &+C_V(\boldsymbol{\sigma}\cdot\hat{\mathbf{R}}')R\cos\theta\cosh(C\mathbf{R}\cdot\mathbf{R}')]\\ &\times\exp\{A\mathbf{R}'^2+B\mathbf{R}^2+D\mathbf{R}^2\cos^2\theta\}. \end{aligned}\tag{12}$$

The total $^3S_1$ amplitude for the longitudinal component is given by

$$\begin{aligned}\hat{T}^{\mathrm{tot}}_{R2}(^3S_1^L) = i\mathcal{N}[&A_L\boldsymbol{\sigma}\cdot\mathbf{R}'\sinh(C\,\mathbf{R}\cdot\mathbf{R}')\\ &+B_L\boldsymbol{\sigma}\cdot\mathbf{R}\cosh(C\,\mathbf{R}\cdot\mathbf{R}')\\ &+C_L(\boldsymbol{\sigma}\cdot\hat{\mathbf{R}}')R\cos\theta\cosh(C\,\mathbf{R}\cdot\mathbf{R}')]\\ &\times\exp\{A\mathbf{R}'^2+B\mathbf{R}^2+D\mathbf{R}^2\cos^2\theta\}\end{aligned}\tag{13}$$

and

$$\begin{aligned}\hat{T}^{\mathrm{tot}}_{R2}(^3S_1^T) = \mathcal{N}[&A_T\boldsymbol{\sigma}\cdot\mathbf{R}'\cosh(C\,\mathbf{R}\cdot\mathbf{R}')\\ &+B_T\boldsymbol{\sigma}\cdot\mathbf{R}\sinh(C\,\mathbf{R}\cdot\mathbf{R}')\\ &+C_T(\boldsymbol{\sigma}\cdot\hat{\mathbf{R}}')R\cos\theta\sinh(C\,\mathbf{R}\cdot\mathbf{R}')]\\ &\times\exp\{A\mathbf{R}'^2+B\mathbf{R}^2+D\mathbf{R}^2\cos^2\theta\}\end{aligned}\tag{14}$$

for the transversal component.

The explicit expressions for the coefficients of Eqs. (12)–(14) are

$$A=-\frac{\alpha(5\alpha+4\beta\gamma^2)}{2(4\alpha+3\beta\gamma^2)},\tag{15a}$$

$$B=-\frac{3(7\alpha^2+18\alpha\beta\gamma^2+9\beta^2\gamma^4)}{8(4\alpha+3\beta\gamma^2)}-D,\tag{15b}$$

$$C=-\frac{3\alpha(\alpha+\beta\gamma^2)}{2(4\alpha+3\beta\gamma^2)},\tag{15c}$$

$$D=-\frac{9\beta(\gamma^2-1)}{8}\left\{1+\frac{\alpha^2}{(5\alpha+4\beta)(5\alpha+4\beta\gamma^2)}\right\},\tag{15d}$$

$$A_V=\frac{\alpha(\alpha+\beta\gamma^2)}{4\alpha+3\beta\gamma^2},\tag{16a}$$

$$B_V=\frac{3(\alpha+\beta\gamma^2)(5\alpha+3\beta\gamma^2)}{2(4\alpha+3\beta\gamma^2)}-C_V,\tag{16b}$$

$$C_V=\frac{3\beta(\gamma^2-1)}{2}\left\{1+\frac{\alpha^2}{(5\alpha+4\beta)(5\alpha+4\beta\gamma^2)}\right\},\tag{16c}$$

$$A_L=-A_V,\tag{17a}$$

$$B_L=\frac{9(\alpha+\beta\gamma^2)^2}{2(4\alpha+3\beta\gamma^2)}-C_L,\tag{17b}$$

$$C_L=\frac{3\beta(\gamma^2-1)}{2}\left\{1-\frac{\alpha^2}{(5\alpha+4\beta)(5\alpha+4\beta\gamma^2)}\right\},\tag{17c}$$

$$A_T=-2A_V,\tag{18a}$$

$$B_T=\frac{3\alpha(\alpha+\beta\gamma^2)}{4\alpha+3\beta\gamma^2}-C_T,\tag{18b}$$

$$C_T=-\frac{3\beta\alpha^2(\gamma^2-1)}{(5\alpha+4\beta)(5\alpha+4\beta\gamma^2)}.\tag{18c}$$

In the nonrelativistic limit $\gamma\to 1$, the results of Ref. [7] are recovered as expected. In particular, the coefficients D, C_V, C_L, and C_T vanish in this limit.

Secondly, we consider the $A2$ diagrams, where the quarks and antiquarks are integrated out similarly to Eq. (7) but where the different flavor-flux topology implies a different momentum transfer. Effectively, this results in one delta function less than for the $R2$ diagram. This will affect the angular dependence and selection rules as will be seen shortly.

We take into account two types of $A2$ diagrams—one in which both $\bar{q}_6q_3$ and $\bar{q}_5q_2$ pairs in Fig. 1(b) annihilate into a $^3S_1$ state, while in the other diagram the $\bar{q}_6q_3$ pair annihilates into the "vacuum" $^3P_0$ state and the $\bar{q}_5q_2$ pair annihilates into the "gluon" $^3S_1$ state followed by the creation of a $\bar{q}_{5'}q_{2'}$ pair. We do not take into account the double $^3P_0$ annihilation since the resulting operator is of the order $\mathcal{O}[(\mathbf{p}/m)^3]$. The integrals for the two cases are

$$\hat{T}_{A2}\left(\frac{^3P_0}{^3S_1},\ \frac{^3S_1}{^3S_1}\right)=\mathcal{N}\int d\mathbf{p}_1 d\mathbf{p}_2 d\mathbf{p}_3 d\mathbf{p}_4 d\mathbf{p}_5 d\mathbf{p}_6 d\mathbf{p}_{1'} d\mathbf{p}_{2'} d\mathbf{p}_{4'} d\mathbf{p}_{5'} \delta(\mathbf{p}_{1'}+\mathbf{p}_{5'}-\mathbf{P}_{\pi^-})\delta(\mathbf{p}_{2'}+\mathbf{p}_{4'}-\mathbf{P}_{\pi^+})\delta(\mathbf{p}_1+\mathbf{p}_2+\mathbf{p}_3-\mathbf{P}_p)$$
$$\times\delta(\mathbf{p}_4+\mathbf{p}_5+\mathbf{p}_6-\mathbf{P}_{\bar{p}})\delta(\mathbf{p}_6+\mathbf{p}_3+\mathbf{p}_1-\mathbf{p}_{1'})\delta(\mathbf{p}_{2'}+\mathbf{p}_{5'}-\mathbf{p}_2-\mathbf{p}_5)\delta(\mathbf{p}_{4'}-\mathbf{p}_4)$$
$$\times\exp\left\{-\frac{1}{4\beta}\left[(\mathbf{p}_{1'}-\mathbf{p}_{5'})^2+(\mathbf{p}_{2'}-\mathbf{p}_{4'})^2+\left(\frac{1}{\gamma^2}-1\right)\{[(\mathbf{p}_{2'}-\mathbf{p}_{4'})\cdot\hat{\mathbf{P}}_\pi]^2+[(\mathbf{p}_{1'}-\mathbf{p}_{5'})\cdot\hat{\mathbf{P}}_\pi]^2\}\right]\right\}$$
$$\times\exp\left\{-\frac{1}{2\alpha}\left(\sum_{i=1}^{3}\left(\mathbf{p}_i-\frac{1}{3}\mathbf{P}_p\right)^2+\sum_{i=4}^{6}\left(\mathbf{p}_i-\frac{1}{3}\mathbf{P}_{\bar{p}}\right)^2\right)\right\}\hat{V}_{A2}\left(\frac{^3P_0}{^3S_1},\ \frac{^3S_1}{^3S_1}\right). \tag{19}$$

The two cases differ only in the operators $\hat{V}_{A2}$ according to the type of annihilation mechanisms used:

$$\hat{V}_{A2}\left(\frac{^3P_0}{^3S_1}\right)=\lambda_{A2P}[\boldsymbol{\sigma}_{63}\cdot(\mathbf{p}_6-\mathbf{p}_3)][\boldsymbol{\sigma}_{52}\cdot\boldsymbol{\sigma}_{2'5'}], \tag{20}$$

$$\hat{V}_{A2}\left(\frac{^3S_1}{^3S_1}\right)=\lambda_{A2S}[-2\ \boldsymbol{\sigma}_{63}\cdot\mathbf{p}_1+i(\boldsymbol{\sigma}_{1'1}\times\boldsymbol{\sigma}_{63})\cdot(\mathbf{p}_1-\mathbf{p}_{1'})]$$
$$\times[\boldsymbol{\sigma}_{52}\cdot\boldsymbol{\sigma}_{2'5'}]. \tag{21}$$

The square brackets above indicate the two exchanges present in the $A2$ diagram in Fig. 1(b). The notation is the same as for the $R2$ diagrams. The strength parameters for $A2$ mechanisms are λ_{A2P} and λ_{A2S}.

Following Fig. 1(b), momentum is transferred from the annihilated $\bar{q}_6 q_3$ pair to quark q_1 (but can also be transferred to $\bar{q}_4$) and from the $\bar{q}_5 q_2$ pair to the created pair $\bar{q}_{5'} q_{2'}$. In r space the $A2$ transition operators for the mixed $^3P_0$ and $^3S_1$ vertices are

$$\hat{T}_{A2}\left(\frac{^3P_0}{^3S_1}\right)=\mathcal{M}[\boldsymbol{\sigma}\cdot\nabla_{R'}+(A_V+B_V)i\boldsymbol{\sigma}\cdot\mathbf{R}]\times\delta(3\mathbf{R}/2-\mathbf{R}')\exp\{(B+D)R^2\} \tag{22}$$

and for two $^3S_1$ annihilation vertices

$$\hat{T}_{A2}\left(\frac{^3S_1}{^3S_1}\right)=\mathcal{M}[\boldsymbol{\sigma}\cdot\nabla_{R'}+(A_L+B_L)i\boldsymbol{\sigma}\cdot\mathbf{R}+(A_T+B_T)\boldsymbol{\sigma}\cdot\mathbf{R}]$$
$$\times\ \delta(3\mathbf{R}/2-\mathbf{R}')\exp\{(B+D)R^2\}. \tag{23}$$

For convenience the relativistic terms B_V, B_L, B_T in the spin coefficients and D in the exponent are written separately from the corresponding nonrelativistic terms A_V, A_L, A_T, and B. All are listed explicitly below.

It is a striking feature of the $A2$ amplitudes that they depend solely on the relative proton-antiproton $\mathbf{R}$ vector but not on the relative orientation of $\mathbf{R}$ and $\mathbf{R}'$. This result is an implicit consequence of Fourier transforming the $A2$ amplitudes to r space, which yields a delta function $\delta(3\mathbf{R}/2-\mathbf{R}')$. One does obtain additional terms due to the relativistic corrections in the pion wave functions, yet these are simpler than for the $R2$ diagrams, and they do not introduce extra angular dependence. Again certain terms, namely, D, B_V, B_L, and B_T, are energy dependent via the boost factor γ. In particular, the exponential factor D is very large (for $\gamma\simeq 7$ it is about 15 times larger than B) and acts like a short-range angle-independent cutoff.

Since the $A2$ diagrams were not discussed in previous work [7], we take the opportunity to analyze their symmetry properties. Taking into account spin-flavor and color matrix elements, the amplitudes in Eqs. (22) and (23) are identical for the permutation of the $A2$ diagram [Fig. 1(b)] in which a $^3P_0$ or $^3S_1$ state resulting from the $\bar{q}_6 q_3$ annihilation is exchanged with $\bar{q}_4$ rather than with q_1. This means that the complete form of $\hat{T}^{\rm tot.}_{A2}$ remains as in Eqs. (22) and (23) and that $\hat{T}_{A2}(^3P_0/^3S_1)$ and $\hat{T}_{A2}(^3S_1/^3S_1)$ are *odd* in $\mathbf{R}$ and $\mathbf{R}'$. Because of the delta function $\delta(3\mathbf{R}/2-\mathbf{R}')$ all $A2$ operators, regardless of the annihilation mechanisms employed, act in $(l_{\pi\pi}\neq l_{\bar{p}p})$ $J^\pi=0^+,1^-,2^+,3^-,4^+,5^-,\ldots$ waves.

We end this section with the expressions for the coefficients of the transition amplitudes (22) and (23):

$$B=-\frac{3(28\alpha^2+36\alpha\beta+9\beta^2)}{8(4\alpha+3\beta)}, \tag{24a}$$

$$D=-9\beta(\gamma^2-1)\left\{1+\frac{4\alpha^2}{(4\alpha+3\beta)(4\alpha+3\beta\gamma^2)}\right\}, \tag{24b}$$

$$A_V=\frac{3(12\alpha^2+14\alpha\beta+3\beta^2)}{2(4\alpha+3\beta)}, \tag{25a}$$

$$B_V=\frac{3\beta(\gamma^2-1)}{2}\left\{1+\frac{4\alpha^2}{(4\alpha+3\beta)(4\alpha+3\beta\gamma^2)}\right\}, \tag{25b}$$

$$A_L=\frac{3(2\alpha+\beta)}{2}, \tag{26a}$$

$$B_L=\frac{3\beta(\gamma^2-1)}{2}, \tag{26b}$$

$$A_T=-\frac{6\alpha(\alpha+\beta)}{4\alpha+3\beta}, \tag{27a}$$

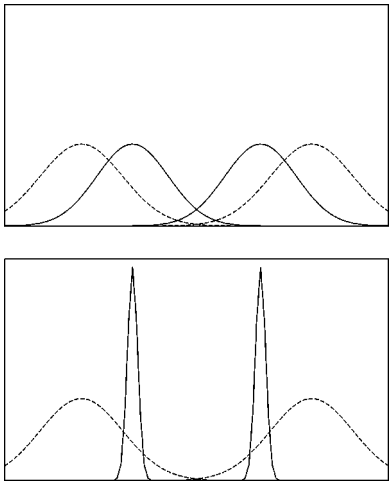

FIG. 2. The first graph shows a two-dimensional projection of the spherical intrinsic pion wave functions (solid lines) given by Eq. (1) and (anti)proton wave functions (dashed lines) of Eq. (2). The distance between the peaks of the solid-line Gaussians represents the relative pion coordinate $\mathbf{R}'=\mathbf{R}_{\pi^-}-\mathbf{R}_{\pi^+}$ whereas the distance between the peaks of the dashed-line Gaussians is the relative $\overline{p}p$ coordinate $\mathbf{R}=\mathbf{R}_{\overline{p}}-\mathbf{R}_p$. The distances remain the same in both graphs. However, in the second graph the boosted intrinsic pion wave function, given by Eq. (5) with $\gamma=7$, is contracted in the boost direction.

$$B_T = -\frac{6\alpha^2\beta(\gamma^2-1)}{(4\alpha+3\beta)(4\alpha+3\beta\gamma^2)}. \tag{27b}$$

Clearly, D, B_V, B_L, and B_T vanish in the nonrelativistic limit $\gamma\to 1$.

IV. GEOMETRIC INTERPRETATION

It is important to understand the geometric implications of deformed pion wave functions as required by relativity and their relation to the $\overline{p}p$ annihilation range. In Sec. I we recall that in a previous (nonrelativistic) attempt to explain the LEAR data on $\overline{p}p\to\pi^-\pi^+$ [2], an increase of proton, antiproton, and pion radii effectively augments the range of the transition operators $\hat{T}_{R2}$ and $\hat{T}_{A2}$. It is therefore surprising that one can obtain any improvement from the Lorentz contraction of pions. After all, we shrink the intrinsic pion wave function in the boost direction, which amounts to less overlap of the quark and antiquark wave functions. The graphic description in Fig. 2 visualizes this. The two intrinsic pion wave functions are plotted at a fixed distance $|\mathbf{R}'|$ from each other and the centers of the (also Gaussian) proton and antiproton intrinsic wave functions are separated by a distance $|\mathbf{R}|$. One sees that, when the pion wave functions are Lorentz contracted in the c.m., the overlap of pions, proton, and antiproton (and of a transition operator depending on the annihilation mechanism, which we omit here for simplicity) decreases considerably and so does their contribution to the annihilation amplitude. Since the total probability is conserved, the Gaussian wave functions of the pions are peaked higher in the lower graph.

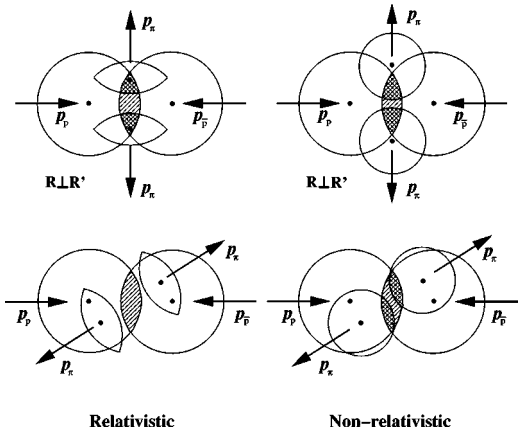

FIG. 3. Sketch of the overlap in the reaction $\overline{p}p\to\pi^-\pi^+$ in the c.m. system at two different angles $\theta_{\text{c.m.}}$ between the incoming $\overline{p}p$ and the outgoing $\pi\pi$ pairs. In the left column, the pions are Lorentz contracted, while in the right column they are described by spherical wave functions. One sees that the angular dependence of the overlaps at the same distances $\mathbf{R}'$ and $\mathbf{R}$ strongly differs in the relativistic and nonrelativistic cases.

As discussed in Sec. III, the $R2$ transition operators acquire new terms which introduce additional angular dependence. The effect of the D term in Eqs. (10) and (11), for example, is strongly angle dependent—for $\mathbf{R}$ parallel or antiparallel to $\mathbf{R}'$, the $\mathbf{R}$ range of $\hat{T}_{R2}$ is drastically reduced due to large D values, whereas for $\mathbf{R}\perp\mathbf{R}'$ this cutoff effect is absent. This angular dependence is schematically depicted in Fig. 3, where $\mathbf{R}'$ and $\mathbf{R}$ have fixed magnitudes. For $\mathbf{R}\perp\mathbf{R}'$ in the top panels one sees that even though the pions are Lorentz contracted, each pion still overlaps with the $\overline{p}p$ pair as in the nonrelativistic case. This overlap vanishes at small angles θ (see lower panels in Fig. 3) and at $\theta=0(\theta=\pi)$ when $\mathbf{R}'$ is (anti)parallel to $\mathbf{R}$. This illustrates that the angle dependence of the overlap in the relativistic and nonrelativistic cases are quite different. That the least overlap occurs for $\mathbf{R}\parallel\mathbf{R}'$ is expressed in the transition operators $\hat{T}_{R2}$ by the $DR^2\cos^2\theta$ term in the exponent of Eqs. (12)–(14). The overlap is minimal at these angles as are the resulting amplitudes $\hat{T}_{R2}$.

The angular momentum content of the scattering matrix elements T^J is obtained by sandwiching the transition operators between the initial-state $\overline{p}p$ and the final-state $\pi^-\pi^+$ wave functions,

$$T^J = \int d\mathbf{R}d\mathbf{R}'\Phi^J_{\pi\pi}(\mathbf{R}')\hat{T}_{R2/A2}(\mathbf{R},\mathbf{R}')\Psi^{J=l\pm1}_{\overline{p}p}(\mathbf{R}), \tag{28}$$

where $\Phi^J_{\pi\pi}(\mathbf{R}')$ and $\Psi^{J=l\pm1}_{\overline{p}p}(\mathbf{R})$ still contain the usual angular dependence in the form of appropriate spherical harmonics. Therefore, additional angle-dependent terms in $\hat{T}_{R2/A2}(\mathbf{R},\mathbf{R}')$ enhance the contribution of higher angular momenta J. The resulting increase of contributions to higher partial waves $J\geqslant 1$ is the main reason for a better description of the experimental data. We will give numerical evidence for this in another communication [20]. A partial wave analysis of the integral in Eq. (28) will show that the richer angular depen-

dence of the $R2$ transition operators considerably increases contributions to partial waves $J=2$ and higher.

V. LORENTZ TRANSFORMATION OF (ANTI)QUARK SPINORS

So far, we have solely treated the Gaussian part of the pion intrinsic wave functions. An s-wave pion wave function in momentum space, omitting flavor and color components, is given by

$$\psi_\pi(\mathbf{p}_i,\mathbf{p}_j) = N_\pi(4\pi/\beta)^{3/2}\delta(\mathbf{p}_i+\mathbf{p}_j-\mathbf{P}_\pi) \times u(\mathbf{p}_i)v(\mathbf{p}_j)\exp\left[-\frac{1}{2\beta}\sum_{\alpha=i,j}\left(\mathbf{p}_\alpha-\frac{1}{2}\mathbf{P}_\pi\right)^2\right]. \tag{29}$$

The momenta $\mathbf{p}_i$ and $\mathbf{p}_j$ denote the antiquark and quark, respectively, $\mathbf{P}_\pi$ is the pion momentum, β is the parameter that determines the size of the pion, and $u(\mathbf{p}_i)$ and $v(\mathbf{p}_j)$ are the usual quark and antiquark Dirac spinors for particles with spin $s=\frac{1}{2}$,

$$u(\mathbf{p},m_s) = \begin{pmatrix} \sqrt{E+m} \\ \dfrac{\boldsymbol{\sigma}\cdot\mathbf{p}}{\sqrt{E+m}} \end{pmatrix}\chi_{m_s}, \tag{30a}$$

$$v(\mathbf{p},m_s) = \begin{pmatrix} \dfrac{\boldsymbol{\sigma}\cdot\mathbf{p}}{\sqrt{E+m}} \\ \sqrt{E+m} \end{pmatrix}\chi_{-m_s}(-)^{1/2-m_s}, \tag{30b}$$

or in terms of helicity spinors

$$u(\mathbf{p},\lambda) = \begin{pmatrix} \sqrt{E+m} \\ \dfrac{2p\lambda}{\sqrt{E+m}} \end{pmatrix}\chi_\lambda(\hat{\mathbf{p}}), \tag{31a}$$

$$v(\mathbf{p},\lambda) = \begin{pmatrix} \dfrac{-2p\lambda}{\sqrt{E+m}} \\ \sqrt{E+m} \end{pmatrix}\chi_{-\lambda}(\hat{\mathbf{p}})(-)^{1/2-\lambda}. \tag{31b}$$

Our approach differs from that of Maruyama *et al.* [15], who use an approximation of the 1s quark wave function in the MIT bag in r space as introduced in Refs. [16,17]. In Ref. [15] the quark wave function is

$$\psi_q(\mathbf{r}_i) = [R_0^3\pi^{3/2}(1+3\zeta^2/2)]^{-1/2}\times\exp\{-r_i^2/2R_0^2\}\begin{pmatrix} 1 \\ i\zeta\dfrac{\boldsymbol{\sigma}\cdot\mathbf{r}_i}{R_0} \end{pmatrix}\chi, \tag{32}$$

where R_0 is the size parameter, which can be related to the bag radius. The parameter ζ determines the probability that the quark is in the *lower* component of the Dirac spinor, and is referred to as the small relativistic component of the wave function. The value of ζ in the bag model has been estimated to be 0.36 for zero quark mass. The authors of Ref. [15] also Lorentz transformed the Gaussian part of the wave function in Eq. (32) into the c.m. but did not apply this transformation to the spinor. In their analysis, Maruyama *et al.* found that the small relativistic components have little influence on the predictions of relative ratios of $\bar{p}p$ annihilation amplitudes into mesons. The effect of including the Lorentz contraction, on the other hand, is to enhance the production of two pions.

In Sec. III, the momentum space transition operators in Eqs. (10), (11), (22), and (23) were calculated making use of just the Gaussian part of the wave function of Eq. (29). In the present section we investigate how Lorentz boosts of quark spinors in the pion wave function of Eq. (29) affect these calculations.

Again, in the pion rest frame S_π the quark four-momentum is p, while in the c.m. frame $S_{\text{c.m.}}$ of the reaction $\bar{p}p\to\pi^-\pi^+$ the quark four-momentum is p'. They are related by the inverse Lorentz transformation $l^{-1}\equiv l^{-1}(\boldsymbol{\beta})$ as follows:

$$p' = l^{-1}p. \tag{33}$$

Here, $\boldsymbol{\beta}=\mathbf{v}/c$ is a vector along the pion momentum $\mathbf{P}_\pi$.

Helicity states in frame S_π are denoted by $|\mathbf{p},\lambda\rangle_{S_\pi}$ while in the c.m. frame $S_{\text{c.m.}}$ they are $|\mathbf{p}',\lambda'\rangle_{S_{\text{c.m.}}}$. The two sets of states are related by

$$|\mathbf{p}',\lambda'\rangle_{S_{\text{c.m.}}} = U(l^{-1})|\mathbf{p},\lambda\rangle_{S_\pi}, \tag{34}$$

where $U(l^{-1})$ is a unitary operator effecting the inverse Lorentz transformation. It can be shown for any Lorentz transformation l that the operation of $U(l)$ on the state $|\mathbf{p},\lambda\rangle$ is equivalent to a rotation $r(l,\mathbf{p})$ in spin space. For a detailed derivation of Lorentz transformations of helicity states, see, for instance, Ref. [18]. The rotations $r(l,\mathbf{p})$ that yield the c.m. states $|\mathbf{p},\lambda\rangle_{S_{\text{c.m.}}}$ are the Wick helicity rotations. With the appropriate $(2s+1)$-dimensional matrix representation $\mathcal{D}^s_{\lambda\lambda'}[r(l,\mathbf{p})]$ where $s=\frac{1}{2}$ is the spin of the (anti)quark, one can rewrite Eq. (34) as

$$|\mathbf{p},\lambda\rangle_{S_\pi}\overset{l^{-1}}{\to}|\mathbf{p}',\lambda'\rangle_{S_{\text{c.m.}}} = \mathcal{D}^s_{\mu\lambda'}[r(l,\mathbf{p})]|l^{-1}\mathbf{p},\mu\rangle_{S_\pi}. \tag{35}$$

A sum over μ is implied. The quark wave functions are obtained from

$$\langle 0|\psi(x)|\mathbf{p},\lambda\rangle = \frac{1}{\sqrt{2\pi}}u(\mathbf{p},\lambda)e^{-ipx}, \tag{36}$$

where $\psi(x)$ is the quark Dirac field. The correspondence $|\mathbf{p},\lambda\rangle\leftrightarrow u(\mathbf{p},\lambda)$ between the physical state and its wave function realization yields the desired Lorentz transformation of the Dirac spinor

$$u(\mathbf{p}',\lambda')_{S_{\text{c.m.}}} = \mathcal{D}^s_{\lambda\lambda'}(r)u(l^{-1}\mathbf{p},\lambda)_{S_\pi}, \tag{37a}$$

and similar arguments lead to

$$v(\mathbf{p}',\lambda')_{S_{\text{c.m.}}} = \mathcal{D}^s_{\lambda\lambda'}(r^{-1})v(l^{-1}\mathbf{p},\lambda)_{S_\pi}. \tag{37b}$$

For the general case of a boost of the axes $l(\boldsymbol{\beta})$, with $\boldsymbol{\beta}=(\beta,\theta_\beta,\phi_\beta)$, the matrices $\mathcal{D}^s_{\lambda\lambda'}$ are

$$\mathcal{D}^{s}_{\lambda\lambda'} = e^{i\eta(\lambda'-\lambda)} d^{s}_{\lambda\lambda'}(\theta_w), \tag{38}$$

where η is a function of the angles θ_β and ϕ_β and the Wick angle θ_w [18] is given by

$$\cos\,\theta_w = \frac{\gamma}{p'}(p + \beta E\,\cos\,\delta). \tag{39}$$

Here, $E=\sqrt{\mathbf{p}^2+m^2}$ is the energy of one (anti)quark as in Eqs. (30a) and (30b), $\gamma = E_{\text{c.m.}}/2m_\pi$, $p=|\mathbf{p}|$, $p'=|l^{-1}\mathbf{p}|$, and $0\leqslant\delta\leqslant\pi$ is the angle between $\mathbf{p}$ and $\boldsymbol{\beta}$, defined by

$$\cos\,\delta = \frac{\boldsymbol{\beta}\cdot\mathbf{p}}{\beta p} = \frac{\mathbf{P}_\pi\cdot\mathbf{p}}{P_\pi p}. \tag{40}$$

For Lorentz boosts $l_z(\boldsymbol{\beta})$, for which the z axis is along $\mathbf{P}_\pi$ in the c.m. system and $\theta_\beta=\phi_\beta=\eta=0$, the expression in Eq. (38) simplifies to

$$\mathcal{D}^{s}_{\lambda\lambda'} = d^{s}_{\lambda\lambda'}(\theta_w). \tag{41}$$

Since $s=\frac{1}{2}$, only two matrix elements are required [19]:

$$d^{1/2}_{1/2,1/2}(\theta_w) = \cos\frac{\theta_w}{2} = \sqrt{\frac{1}{2}+\frac{1}{2}\cos\,\theta_w}$$
$$= \sqrt{\frac{1}{2}+\frac{\gamma}{2p'}(p+\beta E\,\cos\,\delta)}, \tag{42a}$$

$$d^{1/2}_{-1/2,1/2}(\theta_w) = \sin\frac{\theta_w}{2} = \sqrt{\frac{1}{2}-\frac{1}{2}\cos\,\theta_w}$$
$$= \sqrt{\frac{1}{2}-\frac{\gamma}{2p'}(p+\beta E\,\cos\,\delta)}. \tag{42b}$$

This means that the quark helicity spinors in $S_{\text{c.m.}}$ are expressed in terms of Dirac spinors in S_π as

$$u(\mathbf{p}',\lambda') = \begin{pmatrix} \sqrt{E+m} \\ \dfrac{|l^{-1}\mathbf{p}|}{\sqrt{E+m}} \end{pmatrix} \chi_{1/2}(\hat{\mathbf{p}}')\, d^{1/2}_{1/2,\lambda'}(\theta_w)$$
$$+ \begin{pmatrix} \sqrt{E+m} \\ \dfrac{-|l^{-1}\mathbf{p}|}{\sqrt{E+m}} \end{pmatrix} \chi_{-1/2}(\hat{\mathbf{p}}')\, d^{1/2}_{-1/2,\lambda'}(\theta_w) \tag{43a}$$

and similarly for the antiquark spinors,

$$v(\mathbf{p}',\lambda') = \begin{pmatrix} \dfrac{-|l^{-1}\mathbf{p}|}{\sqrt{E+m}} \\ \sqrt{E+m} \end{pmatrix} \chi_{-1/2}(\hat{\mathbf{p}}')\, d^{1/2}_{\lambda',1/2}(\theta_w)$$
$$- \begin{pmatrix} \dfrac{|l^{-1}\mathbf{p}|}{\sqrt{E+m}} \\ \sqrt{E+m} \end{pmatrix} \chi_{1/2}(\hat{\mathbf{p}}')\, d^{1/2}_{\lambda',-1/2}(\theta_w). \tag{43b}$$

To obtain the above expression for antiquark spinors the property $d_{\lambda\lambda'}(-\theta_w)=d_{\lambda'\lambda}(\theta_w)$ has been used. Note that the spinors now depend on T_{lab} via the relativistic factor γ present in Eqs. (42a) and (42b) as well as in the Lorentz boost l^{-1}.

VI. RELATIVISTIC SPINOR CORRECTIONS TO R2 AND A2 DIAGRAMS

Having shown in Sec. III how the Lorentz transformation of the spatial part of the intrinsic pion wave function alters the annihilation operators, we will now discuss the effect on the operators due to modifications in the spinors of the final quarks $i=1',2'$ and antiquarks $i=4',5'$. The $A2$ and $R2$ spin-matrix elements read schematically

$$M_S = \sum_{\{\lambda_i\}=-1/2}^{+1/2} \langle[s_{1'}s_{5'}]_{s_\pi=0}| \otimes \langle[s_{2'}s_{4'}]_{s_\pi=0}|$$
$$\times\, \hat{V}_{R2/A2} |[s_1 s_2 s_3]_{s_p=1/2}\rangle \otimes |[s_4 s_5 s_6]_{s_{\bar{p}}=1/2}\rangle, \tag{44}$$

where $\hat{V}_{R2/A2}$ is either one of the four operators introduced in Eqs. (8), (9), (20), and (21). As before, we neglect relativistic corrections to the $\overline{pp}$ wave functions; hence, only the final quark and antiquark helicity states are Lorentz transformed. Note that the operators $\hat{V}_{R2/A2}$ mentioned above are in the c.m. frame, where they act between initial- and final-state spin wave functions.

In the derivation of the transition operators in Eqs. (8), (9), (20), and (21), only leading order terms in $\mathbf{p}$ were kept. Here the same strategy is followed: we make use of Eqs. (43a) and (43b) but we do apply these boosts to the Pauli spinors in the pions, each consisting of a quark i and antiquark j with spin states $|s_i m_i\rangle$ and $|s_j m_j\rangle$ (with corresponding helicities λ_i and λ_j) and $m_i\neq m_j=\pm 1/2$:

$$|s_\pi = m^z_\pi = 0\rangle = \frac{1}{\sqrt{2}}(|s_i m_i\rangle \otimes |s_j m_j\rangle - |s_i m_j\rangle \otimes |s_j m_i\rangle).$$

The Pauli spinors in the c.m. frame are expressed in terms of the Pauli spinors in S_π by

$$\chi_{\lambda'}(\hat{\mathbf{p}}') = d^{1/2}_{1/2,\lambda'}(\theta_w)\chi_{1/2}(\hat{\mathbf{p}}') + d^{1/2}_{-1/2,\lambda'}(\theta_w)\chi_{-1/2}(\hat{\mathbf{p}}') \tag{45a}$$

for particles and

$$\chi_{\lambda'}(\hat{\mathbf{p}}') = d^{1/2}_{\lambda',1/2}(\theta_w)\chi_{1/2}(\hat{\mathbf{p}}') + d^{1/2}_{\lambda',-1/2}(\theta_w)\chi_{-1/2}(\hat{\mathbf{p}}') \tag{45b}$$

for antiparticles.

The Pauli matrices $\boldsymbol{\sigma}$ in the transition operators $\hat{V}_{R2/A2}$ act on the boosted spinors χ^i_λ, with $i=1',2',4',5'$. The spin-matrix elements pertinent to the $\hat{V}_{R2/A2}$ operators are thus modified since the rotation matrix elements $d^{1/2}_{\pm 1/2,1/2}(\theta_w)$ in Eqs. (42a) and (42b) come into play. We make use of the fact that in the c.m. frame the transverse components of the quark momenta are much smaller than the component along the boost direction (from now on we refer only to the quark but the discussion is identical for the antiquark). We can thus approximate

$$|l^{-1}(\boldsymbol{\beta})\mathbf{p}| = \sqrt{p_\perp^2 + \gamma^2(p_\parallel + \beta E)^2} \simeq \gamma(\mathbf{p}\cdot\hat{\mathbf{P}}_\pi + \beta E), \tag{46}$$

which we write as $p'\simeq\gamma(p\,\cos\,\delta+\beta E)$. This approximation is valid except for a small region where $\cos\,\delta=-\beta E/p$. With

this, the following approximation for the matrix elements $d^{1/2}_{\pm 1/2,1/2}(\theta_w)$ holds:

$$d^{1/2}_{\pm 1/2,1/2}(\theta_w) \simeq \sqrt{\frac{1}{2} \pm \frac{1}{2}\frac{p+\beta E\cos\delta}{p\cos\delta+\beta E}}. \tag{47}$$

The numerator and denominator in Eq. (47) are very similar and the matrix elements $d^{1/2}_{\pm 1/2,1/2}(\theta_w)$ are functions of β rather than of γ.

To illustrate the role of the cos δ term in Eq. (47), we consider two cases cos $\delta = \pm 1$, i.e., for which the quark momentum is parallel or antiparallel to the boost direction $\boldsymbol{\beta}$. Recall that for cos $\delta = \pm 1$, of course, $\mathbf{p}$, vanishes, in which case Eqs. (46) and (47) are exact.

The following relationships exist between helicity and momentum orientation of a quark in the c.m. frame:

$$\text{If } \cos\delta = +1 \begin{cases} d^{1/2}_{1/2,1/2}(\theta_w) = 1, \\ d^{1/2}_{-1/2,1/2}(\theta_w) = 0. \end{cases} \tag{48}$$

In other words, if the quark momentum in the pion rest frame is aligned with the boost direction, then helicity is conserved under the boost. In this case there is no Wick rotation and $\theta_w = 0$. Of course the momentum $\mathbf{p}'$ and boost vector $\boldsymbol{\beta}$ will also be parallel in the c.m. frame.

However, if momentum in the pion rest frame is antiparallel to the boost direction $\boldsymbol{\beta}$ then helicity in the c.m. frame can flip, as seen from Eq. (49) and now $\theta_w = \pi$.

$$\text{If } \cos\delta = -1 \begin{cases} d^{1/2}_{1/2,1/2}(\theta_w) = 0, \\ d^{1/2}_{-1/2,1/2}(\theta_w) = 1. \end{cases} \tag{49}$$

The relativistic effect described in Eqs. (48) and (49) can be interpreted as follows. Assume a quark inside the pion with a given helicity and its momentum oriented antiparallel to the boost direction $\boldsymbol{\beta}$. For very large boosts, an observer in the c.m. system perceives a reversed quark momentum. As the spin direction is not changed, this implies a flipping of the helicity in the c.m. frame, which confirms that for cos $\delta = -1$ the matrix element $d^{1/2}_{1/2,1/2}(\theta_w)$ is zero whereas $d^{1/2}_{-1/2,1/2}(\theta_w)$ is 1 as seen in Eq. (49). On the other hand, if the quark momentum in the pion frame is parallel with $\boldsymbol{\beta}$, then helicity will not flip, as the quark momentum in the c.m. is still seen in the boost direction and $d^{1/2}_{-1/2,1/2}(\theta_w)$ must be zero in agreement with Eq. (48). Hence, helicities can flip from one reference frame to the other depending on the initial orientation of the quark momentum with respect to the boost direction.

For intermediate angles $-1 \leqslant \cos\delta \leqslant +1$, Eqs. (45a) and (45b) describe the degree of helicity flip due to the change of reference frame. Since the rotation matrices are proportional to β, the relativistic effects from the spinors tend to be much smaller than those from the spatial components discussed previously in Sec. III.

VII. CONCLUSION

In this paper, the effects of Lorentz transformations on intrinsic pion wave functions in the reaction $\bar{p}p \to \pi^-\pi^+$ are investigated. This is done within the framework of a constituent quark model used previously [2,7,8] to describe $d\sigma/d\Omega$ and A_{0n} data of this reaction. The Lorentz transformations are effected on both the spatial part as well as the quark spinor components in the intrinsic pion wave functions. We find that the coordinate-space wave function is strongly contracted along the boost direction, and that the spatial part of the annihilation amplitudes depends on γ and γ^2. The spinors are modified by Wick rotations and the relativistic effects due to spin are therefore proportional to β rather than to the boost factor γ.

In addition to the nonplanar quark rearrangement diagrams $R2$, we also compute the transition operators originating from the planar $A2$ diagrams for pure $^3S_1$ as well as a mixture of $^3S_1$ and $^3P_0$ annihilation mechanisms.

The nonrelativistic annihilation operator for the nonplanar $R2$ diagrams was given in Ref. [7]. In this paper, we obtain new terms in the operator that affect its range and introduce additional angular dependence. The dependence on the c.m. energy $\sqrt{s}$ is now manifest via the relativistic boost factor γ. Most of the new relativistic factors are considerably larger than the nonrelativistic ones. Therefore, the geometry of the annihilation amplitudes is drastically modified. Nonetheless, the selection rules described in Ref. [7] are preserved. The $A2$ amplitudes are simpler than the $R2$ amplitudes, and they depend only on the relative distance of the proton and antiproton.

We will show [20] that the modifications in the annihilation amplitudes, due to relativistic considerations, strongly improve the description of the cross section and analyzing power as measured at LEAR [1]. Therefore with a relativistic treatment one obtains a description of the reaction $\bar{p}p \to \pi^-\pi^+$ similar to or better than with the *ad hoc* increase of the particle radii which was the approach in Ref. [7].

ACKNOWLEDGMENTS

B.E. would like to thank Benoît Loiseau for helpful discussions and the Laboratoire de Physique Nucléaire et de Hautes Energies (Groupe Théorie) at the Université Pierre et Marie Curie for its hospitality and support. Part of this work was carried out at the Institute for Nuclear Theory, University of Washington, to whom he is grateful for a welcoming atmosphere and support during his stay. W.M.K. acknowledges a very stimulating discussion with Stefan Scherer. The effects of Lorentz transformations of spinors were investigated due to stimulating comments by Ronald Gilman.

[1] A. Hasan *et al.*, Nucl. Phys. **B378**, 3 (1992).
[2] B. El-Bennich, W. M. Kloet, and B. Loiseau, Phys. Rev. C **68**, 014003 (2003).
[3] W. M. Kloet and F. Myhrer, Phys. Rev. D **53**, 6120 (1996).
[4] B. Moussallam, Nucl. Phys. **A407**, 413 (1983); **A429**, 429 (1984).
[5] V. Mull, J. Haidenbauer, T. Hippchen, and K. Holinde, Phys. Rev. C **44**, 1337 (1991).
[6] V. Mull, K. Holinde, and J. Speth, Phys. Lett. B **275**, 12 (1992).
[7] G. Bathas and W. M. Kloet, Phys. Lett. B **301**, 155 (1993).
[8] G. Bathas and W. M. Kloet, Phys. Rev. C **47**, 2207 (1993).
[9] Y. Yan and R. Tegen, Phys. Rev. C **54**, 1441 (1996); Nucl. Phys. **A648**, 89 (1999).
[10] A. M. Green and J. A. Niskanen, Nucl. Phys. **A412**, 448 (1984).
[11] A. M. Green and J. A. Niskanen, Nucl. Phys. **A430**, 605 (1984).
[12] C. B. Dover, T. Gutsche, M. Maruyama, and A. Faessler, Prog. Part. Nucl. Phys. **29**, 87 (1992).
[13] S. Amendolia *et al.*, Nucl. Phys. **B277**, 168 (1986).
[14] F. Borkowski *et al.*, Nucl. Phys. **B93**, 461 (1975).
[15] M. Maruyama, T. Gutsche, A. Faessler, and G. L. Strobel, Phys. Rev. C **42**, 716 (1990).
[16] I. Duck, Phys. Lett. **77B**, 223 (1978).
[17] C. W. Wong, Phys. Rev. D **24**, 1416 (1981).
[18] E. Leader, *Spin in Particle Physics* (Cambridge University Press, Cambridge, U.K., 2001), pp. 18–33.
[19] D. M. Brink and G. R. Satchler, *Angular Momentum*, 3rd ed. (Oxford University Press, Oxford, 1994), p. 24.
[20] B. El-Bennich and W. M. Kloet, nucl-th/0403071.